Journal of
Nanoscience and Nanotechnology
Vol. 13, 1–7, 2013

Transparent Anodic TiO_2 Nanotube Arrays on Plastic Substrates for Disposable Biosensors and Flexible Electronics

Samira Farsinezhad[1], Arash Mohammadpour[1], Ashley N. Dalrymple[1], Jared Geisinger[1], Piyush Kar[1], Michael J. Brett[1,2], and Karthik Shankar[1,*]

[1] *Department of Electrical and Computer Engineering, University of Alberta, Edmonton, AB, T6G 2V4, Canada*
[2] *National Institute for Nanotechnology, National Research Council, 11421 Saskatchewan Drive, Edmonton, AB, T6G 2M9, Canada*

Exploitation of anodically formed self-organized TiO_2 nanotube arrays in mass-manufactured, disposable biosensors, rollable electrochromic displays and flexible large-area solar cells would greatly benefit from integration with transparent and flexible polymeric substrates. Such integration requires the vacuum deposition of a thin film of titanium on the desired substrate, which is then anodized in suitable media to generate TiO_2 nanotube arrays. However the challenges associated with control of Ti film morphology, nanotube array synthesis conditions, and film adhesion and transparency, have necessitated the use of substrate heating during deposition to temperatures of at least 300 °C and as high as 500 °C to generate highly ordered open-pore nanotube arrays, thus preventing the use of polymeric substrates. We report on a film growth technique that exploits atomic peening to achieve high quality transparent TiO_2 nanotube arrays with lengths up to 5.1 μm at room temperature on polyimide substrates without the need for substrate heating or substrate biasing or a Kauffman ion source. The superior optical quality and uniformity of the nanotube arrays was evidenced by the high specular reflectivity and the smooth pattern of periodic interferometric fringes in the transmission spectra of the nanotube arrays, from which the wavelength-dependent effective refractive index was extracted for the air-TiO_2 composite medium. A fluorescent immunoassay biosensor constructed using 5.1 μm-long transparent titania nanotube arrays (TTNAs) grown on Kapton substrates detected human cardiac troponin I at a concentration of 0.1 μg ml^{-1}.

Keywords: Transparent, Metal Oxide, Anodization, Self-Organized, Thin Film Deposition, Polymer Substrates, Atomic Peening, Troponin Biomarker Assay.

RESEARCH ARTICLE

1. INTRODUCTION

The three major classes of porous nanomaterials that are curently the subject of intense research activity are: microporous metal-organic frameworks (MOFs), which primarily consist of pore sizes < 2 nm,[1] mesoporous materials with pore-sizes in the range 2–50 nm[2,3] and nanoporous materials which consist of pores 20–200 nm in size. Among nanoporous materials, anodically formed self-organized TiO_2 nanotube arrays have an extremely versatile application spectrum[4–6] ranging from biomedical devices through electrochromic and photovoltaic devices to catalysts, separation membranes and chemical sensors, enabled by the following properties: a high surface area, ordered pore architecture, *n*-type semiconductive behavior when crystallized, well-defined percolation pathways for charge carriers and tunability of the diameter,[7,8] tube-length, wall-thickness and effective refractive index over a wide size range, and high refractive index. Specific applications for titania nanotube arrays include stem-cell differentiators,[9,10] drug-eluting osteogenic impants,[11] ultrasensitive immunoassays,[12,13] amperometric sensors,[14–16] biofiltration membranes,[17] electrochromic displays,[18,19] oxidative photocatalysts for the degradation of organic contaminants,[20] reductive photocatalysts for conversion of CO_2 into hydrocarbon fuels,[21,22] photoanodes for sunlight-driven water splitting,[23,24] supercapacitor electrodes in energy storage devices[25] and electron-collection scaffolds for dye-sensitized and ordered bulk heterojunction solar cells.[26–28] Several of the above mentioned applications rely

*Author to whom correspondence should be addressed.

on the propagation of light through the nanotubes. In this regard, native titanium metal foils, which are the most commonly used substrate for the growth of TiO_2 nanotube arrays are severely limiting due to their non-transparency. For instance, backside illumination is inefficient in TiO_2 nanotube-based dye-sensitized (bulk heterojunction) solar cells due to optical absorption losses through the counter-electrode (anode) and redox electrolyte (hole transporter). Frontside illumination uses light more efficiently and requires TiO_2 nanotubes on a transparent substrate. For low-cost applications in sensing and organic electronics, flexible polymeric substrates are highly desirable. Scaling up the fabrication of uniform nanotube arrays to substrates of larger areas is an ongoing endeavour.[29] Previous studies have investigated the effect of process variables that directly affect the quality of the nanotubes formed, namely the substrate temperature during deposition, the stress mismatch of the substrate and Ti films and the film thickness. Based on these studies, current methods for generating highly ordered TTNAs with unclogged pores on large area non-native substrates for use in high-performance devices rely on substrate heating during the vacuum deposition of thin films of titanium, which are subsequently anodized to form TTNAs.[30–33] The use of substrate heating in these reports to temperatures of 300 °C–500 °C precludes the use of flexible polymeric substrates. TTNAs on glass and Si substrates have also been realized by recourse to more complex deposition tools utilizing substrate biasing and/or ion-beam sputtering.[34, 35] Recently, a number of reports have reported TTNA formation on transparent and flexible substrates using direct current and radio-frequency sputtering processes at low temperature[36–38] but the quality of the nanotubes obtained are not optimal. Pore clogging even after ultrasonication is evident in several of these reports.[36] Sverbeglieri et al.[39] required an ink-pen pre-treatment of the Ti layer before anodization to obtain TTNAs on Kapton with a debris-free surface. Secondly, the optical properties of such low temperature grown TTNAs have been inadequately characterized. Thirdly, none of these reports have used the TTNAs in optical biosensors, an important class of applications for transparent, flexible titania nanotube arrays.[40] Figure 1 shows self-organized TTNAs with open pores on bendable Kapton films, obtained by anodizing Ti films deposited by direct current magnetron sputtering at room temperature without any pre-treatment. The nanotubes are ordered, completely free of debris and similar in quality to nanotubes obtained on Ti foil substrates. In addition, we

(i) explain the atomic peening mechanism that allows us to forego substrate heating,

(ii) obtain the effective refractive index of the TTNAs over a wide wavelength range by optical measurements and

(iii) obtain proof of concept results demonstrating the use of TTNAs in fluorescence immunoassays.

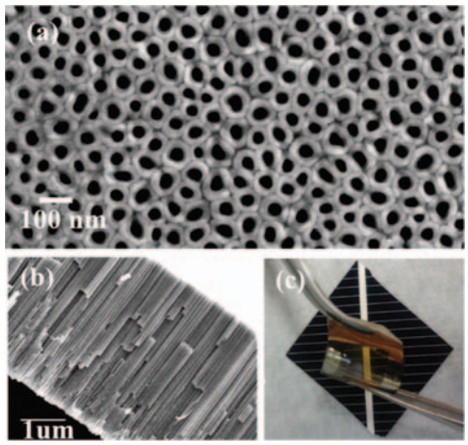

Fig. 1. (a) Top-view and (b) cross-section of 5.1 μm TiO_2 nanotube arrays on 50 μm thick Kapton® substrate, and (c) flexible and transparent TiO_2 nanotube arrays on Kapton®; the substrate in the background is a silicon solar cell.

2. EXPERIMENTAL DETAILS

2.1. Thin Film Deposition

50 μm-thick Dupont Kapton type E substrates were consecutively degreased ultrasonically in solutions of micro-90 concentrated cleaning solution (Sigma-Aldrich), DI water and isopropanol. Titanium thin film deposition was performed at room temperature in a Kurt Lesker DC magnetron sputtering system using Argon gas at a power of 150 W and at pressures ranging from 7 mtorr to 1 mtorr.

2.2. Anodic Growth of TiO_2 Nanotube Arrays

Parafilm windows were sealed on to 2.5 cm × 1.2 cm strips of Ti-coated Kapton to expose areas of $\sim$1 cm^2 for electrochemical anodization. The sample was connected with the electrolyte by an O-ring to form the anode while the cathode consisted of a graphite rod 3 mm in diameter. The distance between the anode and the cathode was approximately 4 cm. A digital DC power supply (MPJA Inc.) was used to drive the reaction at room temperature. The anodization electrolyte contained 0.3 wt% NH_4F and 4 vol% deionized water in ethylene glycol. Potentiostatic anodization was performed at 40 V and the anodization current was monitored and recorded using a Keithley 4200-SCS semiconductor parameter analyzer. The endpoint of the anodization was detected by a drop in current and by the Ti-coated Kapton turning transparent. No trace of metallic Ti was observed under the titania nanotube arrays. Subsequently, the sample was immersed in ethanol for 30 s and dried using a nitrogen gun. Volume expansion associated with the transformation of metallic titanium to titanium dioxide resulted in 900 nm and 5.1 um thick nanotube arrays from 500 nm and 2 um thick titanium films respectively.

2.3. Immunoassay Protocols

The protocols have been more extensively explained elsewhere.[13] Briefly, TiO_2 nanotube arrays on Kapton were immersed overnight in a 1 mM solution of PHA in a 4:1 mixture of ethanol and water. The COOH groups on the monolayer were activated by EDC/NHS coupling and conjugated to 20 μg ml^{-1} polyclonal anti-goat troponin in phosphate buffer solution (PBS) in 1 hour. A one hour immersion in 1% Bovine Serum Albumin (BSA) in PBS was used to block unreacted carboxylic acid groups. Samples were then exposed to troponin solutions of defined concentrations for 2 hours. Following troponin capture, samples were incubated for 30 min in a 20 μg ml^{-1} solution of monoclonal secondary antibody, namely anti-mouse troponin in PBS buffer. Finally, surface-bound secondary antibody was tagged by binding to anti-mouse fluorescence (AM700).

2.4. Characterization

The morphology of the samples was images using a cold cathode JEOL 6301F field-emission scanning electron microscope. Optical measurements on the samples were performed using a Perkin Elmer Lambda 900 UV-Vis-NIR spectrophotometer. Fluorescence imaging was performed using an Odyssey Imager (Li-Cor Biosciences), a two channel laser-based near-infrared detection system.

3. RESULTS AND DISCUSSION

The characteristics of Ti film growth exercise a large influence on the morphology, uniformity, and shape and size dispersity of the TiO_2 nanotube arrays that result following electrochemical anodization. Using Auger electron spectroscopy and other techniques, the Ti film growth mode on a variety of surfaces including polyimide, single-crystal silicon, tungsten, etc. has been determined to be of the Stranski-Krastanov type consisting of the formation of a complete first monolayer of Ti atoms followed by the growth of three-dimensional islands.[41] The low adatom mobility of Ti atoms on oxygen-terminated surfaces such as glass and tin oxide derivatives as well as on carbonyl group-terminated surfaces such as polyimide[41] limits the surface diffusion of Ti atoms in the growing Ti film, and the high melting point of Ti limits self-diffusion. The resulting columnar growth consists of grain growth primarily in the direction perpendicular to the substrate with a much smaller increase in lateral dimensions of the grains. Columnar growth is also characterized by the build-up of only tensile stress which increases with film thickness and results in the adhesion problems noted by several researchers, particularly for thick Ti films. Substrate heating provides more adatom mobility to Ti atoms and allows for the formation of platelets and better filling of the inter-island spaces. In a series of studies, Kalantar-Zadeh et al.[42–44] have clearly shown using deposition pressures of 20 mtorr and radio-frequency sputtering, that Ti films deposited at high temperatures form ordered flatter hexagonal grains conducive to uniform pitting during the early stages of the anodization process to form TTNAs while Ti films deposited at room temperature form columnar grains that nucleate pits inhomogeneously and with random orientations, and are furthermore subject to lateral etching at the grain boundaries during anodization. Films deposited at room temperature were also found to have poor adhesion and delaminated soon after immersion in the anodization electrolyte.[31]

To obtain Ti films with a uniform morphology and good adhesion, we used low-pressure DC magnetron sputtering of titanium in an argon ambient onto substrates held at room temperature. Figure 2 shows the morphologies of 500 nm-thick Ti films deposited at room temperature on Kapton by direct current magnetron sputtering at two different argon pressures, 7 mtorr and 1 mtorr. The films deposited at 7 mtorr possess high porosity and surface roughness due to the growth of large columnar three-dimensional grains. The films deposited at 1 mtorr, on the other hand, are relatively smooth and uniform due to the positive effect of atomic peening.[45] At low deposition pressures, the Ti atoms ejected from the target have longer mean free paths and arrive at the substrate with greater kinetic energy. Simultaneously, Ar^+ ions are neutralized at the cathode and reflected from it. The reflected neutrals collide more frequently with the substrate. Both processes increase adatom mobility in the growing film and simulate the effect of substrate heating, while also improving intermixing between the uppermost atomic layers of the substrate and the first few atomic layers of the growing film, thus inducing superior adhesion. Atomic peening also

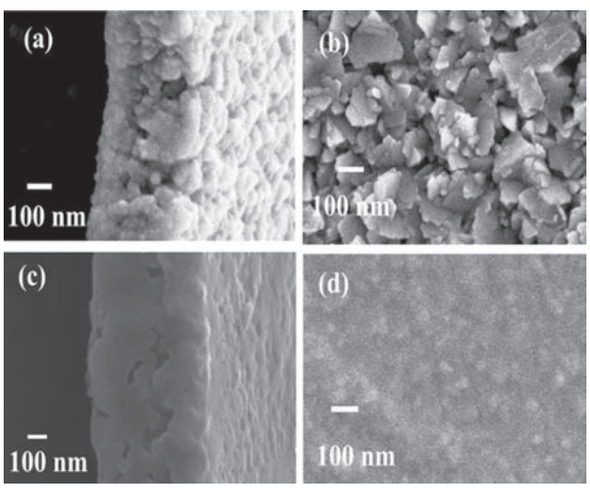

Fig. 2. (a), (b) Top-view and cross-section respectively of a 500 nm thick film of Ti sputtered on to unheated Kapton® substrates at a chamber pressure of 7 mtorr, and (c), (d) Top-view and (d) cross-section respectively of a 500 nm thick film of Ti sputtered on to unheated Kapton® substrates at a chamber pressure of 1 mtorr.

RESEARCH ARTICLE

densifies the films by packing them more closely into the film and by forcing atoms into tiny, hard to reach spaces, a process otherwise impossible under conditions of thermal equilibrium.[46] The microstructure and compactness of the Ti film improves due to the energetic particle bombardment and the atomic peening mechanism causes an underlying change in the deposition process. Consequently, the void portion is decreased and the resulting films are more uniform as in Figures 2(c) and (d).

During electrochemical anodization of the vacuum deposited metal film, the interplay between the three competing processes of field-asssisted oxidation of the Ti, field assisted dissolution of the oxide and chemical dissolution of the oxide, determines the evolution of the morphology and the formation of TiO_2 nanotube arrays. The two field-assisted processes have currents associated with them that are observable in the anodization current transient (Fig. 3) while chemical etching is much weaker and has a relatively minor effect in the organic anodization electrolytes used by us in this work. In Figure 3(a), the sharp decrease in current at the onset of anodization is due to the formation of an insulating barrier layer of TiO_2 by field-assisted oxidation. In films deposited by a peening-assisted process, field-assisted dissolution nucleates uniform pits in the compact insulating oxide causing an increase in the anodization current until a local maximum is reached. Subsequently, the barrier layer thickness increases very slowly as the processes of pore self-organization and propagation occur during a steady decrease of the anodization current with time. In highly porous, non-uniform Ti films consisting of three-dimensional grains, pits oriented in several different directions are nucleated as opposed to only pits orthogonal to the substrate, and therefore interferes with the self-organization process to yield less ordered poorer quality nanotubes, and in some cases a mere irregular nanoporous structure is obtained. As the anodization process reaches completion (defined by the near complete conversion of the Ti film into a TiO_2 nanotube array), the conductive Ti film at the bottom of the nanotube array thins out and the anodization current undergoes a steep decrease due to the concomitant increase in resistance. The resulting nanotubes are transparent as shown in Figure 1(c).

For light propagation, the titanium dioxide nanotube array may be modeled as an effective medium consisting of TiO_2 with air inclusions. Due to the difference in optical path length between light reflected at the TNA-barrier layer interface and the TNA-air interface, Fabry-Perot

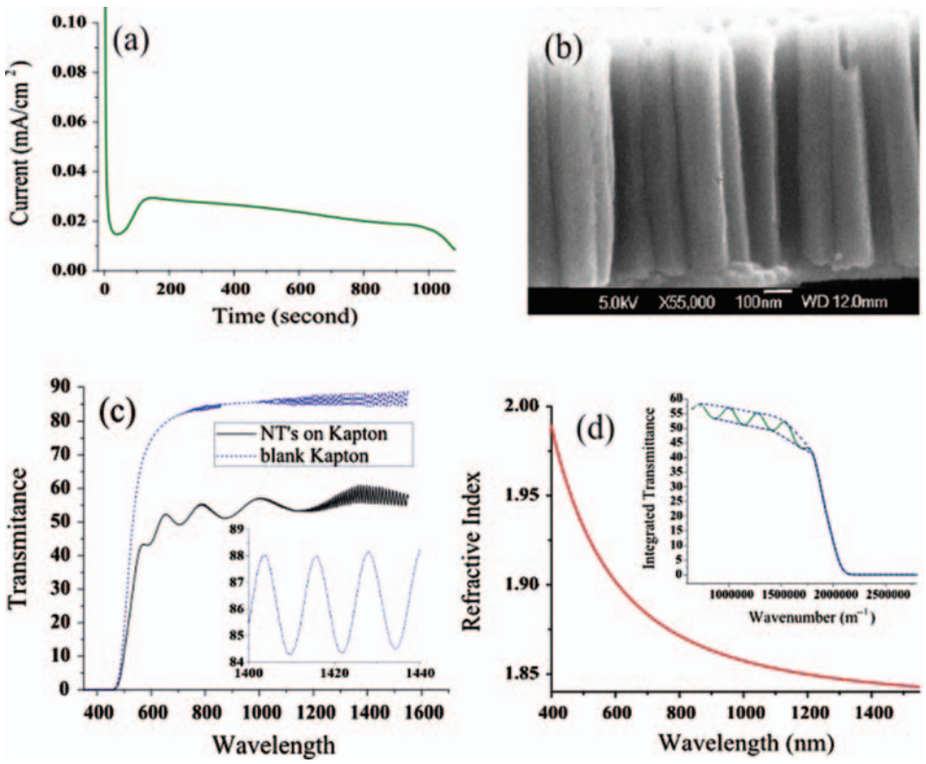

Fig. 3. A 500 nm Ti film on Kapton was formed by sputtering at a chamber pressure of 1 mtorr and subjected to electrochemical anodization in a fluoride ion bearing water-ethylene glycol electrolyte to form TiO_2 nanotube arrays. (a) Anodization current versus time (b) cross-sectional FESEM image showing a film thickness (i.e., tube-length) of 870 nm (c) optical transmittance of blank Kapton substrates (blue curve) and TiO_2 nanotubes on Kapton (black curve) with the inset showing the Fabry-Perot interference fringes of the blank Kapton substrate in more detail and (d) effective refractive index of the nanotube arrays on Kapton, calculated by applying the envelope to the transmission spectra as shown in the inset.

RESEARCH ARTICLE

interference fringes are expected in the reflectance and transmission spectra, given by

$$d = \frac{\lambda_1 \lambda_2}{2(\lambda_1 n_2 - \lambda_2 n_1)} \quad (1)$$

where d is the film thickness and the refractive indices of the film corresponding to adjacent maxima (or minima) at points 1 and 2 are given as n_1 at λ_1 and n_2 at λ_2. Non-uniformities in the TiO_2 nanotube array film such as high surface roughness or differences in the height of individual nanotubes generate optical scattering, that reduces the distinctness of the fringe pattern. Figure 3(c) shows that room-temperature fabricated TiO_2 nanotube arrays show a clear pattern of interference fringes at visible wavelengths, indicating the high quality of the nanotubular film. Due to the small optical thickness of the Kapton substrates (47.5 μm thick), the substrate also produces interference fringes at infrared wavelengths (inset of Fig. 3(c)) which complicates the analysis of the optical properties of the film. Furthermore, Kapton substrates strongly absorb photons of wavelengths 500 nm and below. We first obtained the wavelength-dependent complex refractive index ($n_s = s - ik_s$) of the Kapton substrates and then used Manifacier's envelope method, modified by Swanepoel and others to account for optically thin and slightly absorbing substrates.[47–49] The resulting envelope function with an upper envelope $T_M(\tilde{U}.)$ and a lower envelope $T_M(\tilde{U})$ is shown in the inset of Figure 3(d) and was used to calculate the effective refractive index $n(\lambda)$ of the nanotube array film in the weak absorption and transparent regions of the transmission spectrum per the relations:

$$n = \sqrt{N + \sqrt{(N^2 - s^2)}} \quad (2)$$

where N is defined by

$$N = 2s\left[\frac{T_M - T_m}{T_M T_m}\right] + \frac{s^2 + 1}{2} \quad (3)$$

The calculated values of n were then fit to a Cauchy dispersion model for extrapolation to shorter wavelengths; these results are shown in Figure 3(d). A film thickness of 940 nm was obtained by application of Eq. (1), which agrees closely with the 870 nm tube-length estimated from the cross-sectional SEM image of Figure 3(b). Using the morphological parameters of the nanotube arrays estimated from the SEM image in Figure 1(a), we calculate a purely geometrical fill-fraction of 63.7% for the TiO_2 phase in the nanotube arrays. For such a two component medium consisting of air and TiO_2, the effective permittivity is given by the Bruggeman effective medium model:

$$f\frac{\varepsilon_{TiO_2} - \varepsilon}{\varepsilon_{TiO_2} - 2\varepsilon} + (1 - f)\frac{1 - \varepsilon}{1 + 2\varepsilon} = 0 \quad (4)$$

where f is the fill-fraction of TiO_2 and $\varepsilon = n^2$ is the effective permittivity of the nanotube array. By substituting the values of the fill-fraction and the calculated effective refractive index of the TiO_2 nanotube arrays shown in Figure 3(d), we obtained a value of 2.4 for the refractive index of the TiO_2 skeleton, which is close to the value for bulk TiO_2. This indicates that the walls of the titania nanotube arrays on Kapton substrates are highly compact and free of air inclusions, useful in generating high refractive index contrast for label-free biosensing approaches based on interferometry.[50]

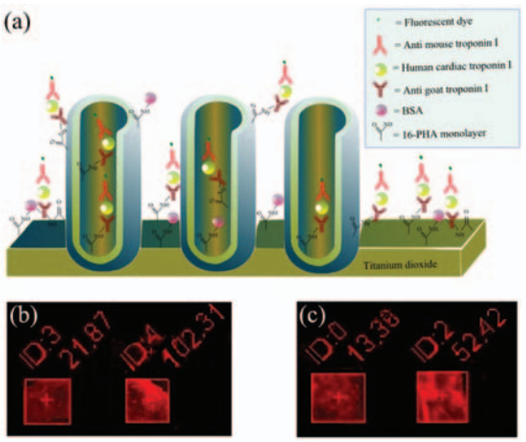

Fig. 4. (a) Schematic illustration of the sandwich-type immunoassay for human cardiac troponin I, (b) Fluorescence micrographs of arrays of 900 nm-long transparent TiO_2 nanotubes on Kapton exposed to left: 0 μg ml^{-1} cTnI (control) and right: 10 μg ml^{-1} cTnI and (c) Fluorescence micrographs of arrays of functionalized arrays of 5 μm-long transparent TiO_2 nanotubes on Kapton exposed to left: 0 μg ml^{-1} cTnI (control) and right: 0.1 μg ml^{-1} cTnI.

The TiO_2 nanotube arrays on Kapton were used to build and test a sandwich immunoassay for human cardiac troponin I (cTnI). Figure 4 shows a schematic of the immunoassay along with the results obtained for nanotubes of two different lengths, 900 nm and 5.1 μm respectively. 16-phosphonohexadecanoic acid (PHA) is a bifunctional molecule consisting of phosphonic acid and carboxylic acid groups at opposite ends of an alkyl chain. PHA was anchored on to the nanotubes through the phosphonic acid headgroup as a self-assembled monolayer. The carboxylic acid headgroup, pointed away from the surface of TiO_2, was used to bind a polyclonal primary troponin-specific antibody, which acted as a capture probe for cTnI. After the troponin binding step, a secondary monoclonal antibody was used to detect the presence of surface bound cTnI and was tagged by binding to a dye-labeled immunoglobulin protein. Biomarker detection was accomplished by comparing the relative fluorescence intensities of a sample exposed to cTnI and a control sample that was never in contact with cTnI. Figure 4(b) shows 900 nm long nanotubes detecting 10 μg ml^{-1} of cTnI with a S/N ratio > 4 while the 5.1 μm-long nanotubes detected 0.1 μg ml^{-1} of cTnI with a S/N ratio of ~ 4 (Fig. 4(c)). One major concern with nanotubes on Kapton substrates for biosensing included the possibility of nanotubes delaminating from the substrate due to capillary force-induced clumping, poor adhesion, internal stresses and phase change initiated by

RESEARCH ARTICLE

prolonged contact with aqueous solution.[51] Other concerns included a larger background fluorescence due to interactions between the Kapton substrate and the bifunctional molecular monolayer. The assays in this report, while not optimized, provided a proof of concept demonstration that the nanotubes on Kapton did not peel off during exposure to buffered solutions containing antibodies and performed effectively as fluorescence biosensors.

4. CONCLUSION

TiO_2 nanotube arrays were successfully grown at room temperature on transparent and flexible substrates made of commercially available polyimide. The Ti films needed for anodization were deposited in a widely available DC sputtering system without the use of substrate heating or substrate biasing or additional ion sources. Longer mean free paths of the sputtered Ti atoms at lower pressures and collisions of the growing film with reflected neutrals produced high quality Ti films at room temperature through atomic peening. A disposable fluorescent immunoassay biosensor based on titania nanotube arrays on Kapton, was demonstrated to be capable of detecting human cardiac troponin I at concentrations as low as 100 ng ml^{-1}.

Acknowledgments: All authors thank NSERC, nanoBridge and the Canada School of Energy and the Environment for funding support. Samira Farsinezhad and Arash Mohammadpour thank Alberta Innovates Technology Futures for scholarship support, and CMC Microsystems for nanofabrication support. Karthik Shankar thanks Suncor for support provided by his PetroCanada Young Innovator Award. Infrastructure used in the project was made available by a Leaders Opportunity Fund grant from the Canada Foundation for Innovation and matched by Alberta Education and Technology to Karthik Shankar. The authors acknowledge the staff at the University of Alberta Nanofab and at the UofA EAS Scanning Electron Microscopy Lab.

References and Notes

1. W. M. Xuan, C. F. Zhu, Y. Liu, and Y. Cui, *Chem. Soc. Rev.* 41, 1677 (**2012**).
2. K. Ariga, A. Vinu, Y. Yamauchi, Q. M. Ji, and J. P. Hill, *Bull. Chem. Soc. Jpn.* 85, 1 (**2012**).
3. I. Nam, N. D. Kim, G. P. Kim, J. Park, and J. Yi, *J. Nanosci. Nanotechnol.* 12, 5704 (**2012**).
4. C. A. Grimes and G. K. Mor, TiO_2 Nanotube Arrays: Synthesis, Properties, and Applications, Springer, New York (**2009**).
5. P. Roy, S. Berger, and P. Schmuki, *Angew. Chem. Int. Ed.* 50, 2904 (**2011**).
6. K. Shankar, TiO_2 nanotube arrays: Growth and application, Encyclopedia of Nanotechnology, edited by B. Bhushan, Springer (**2012**).
7. A. Mohammadpour, P. R. Waghmare, S. K. Mitra, and K. Shankar, *ACS Nano* 4, 7421 (**2010**).
8. A. Mohammadpour and K. Shankar, *J. Mater. Chem.* 20, 8474 (**2010**).
9. S. Oh, K. S. Brammer, Y. S. J. Li, D. Teng, A. J. Engler, S. Chien, and S. Jin, *Proc. Natl. Acad. Sci. U.S.A.* 106, 2130 (**2009**).
10. J. Park, S. Bauer, P. Schmuki, and K. von der Mark, *Nano Lett.* 9, 3157 (**2009**).
11. K. C. Popat, M. Eltgroth, T. J. LaTempa, C. A. Grimes, and T. A. Desai, *Biomaterials* 28, 4880 (**2007**).
12. Y.-Y. Song, F. Schmidt-Stein, S. Berger, and P. Schmuki, *Small* 6, 1180 (**2010**).
13. P. Kar, A. Pandey, J. J. Greer, and K. Shankar, *Lab on a Chip* 12, 821 (**2012**).
14. S. Q. Liu and A. C. Chen, *Langmuir* 21, 8409 (**2005**).
15. P. Xiao, B. B. Garcia, Q. Guo, D. W. Liu, and G. Z. Cao, *Electrochem. Commun.* 9, 2441 (**2007**).
16. X. Y. Pang, D. M. He, S. L. Luo, and Q. Y. Cai, *Sens. Actuator B-Chem.* 137, 134 (**2009**).
17. M. Paulose, L. Peng, K. C. Popat, O. K. Varghese, T. J. LaTempa, N. Z. Bao, T. A. Desai, and C. A. Grimes, *J. Membr. Sci.* 319, 199 (**2008**).
18. R. Kirchgeorg, S. Berger, and P. Schmuki, *Chem. Commun.* 47, 1000 (**2011**).
19. Y. Y. Song, Z. D. Gao, J. H. Wang, X. H. Xia, and R. Lynch, *Adv. Funct. Mater.* 21, 1941 (**2011**).
20. K. Shankar, J. I. Basham, N. K. Allam, O. K. Varghese, G. K. Mor, X. J. Feng, M. Paulose, J. A. Seabold, K. S. Choi, and C. A. Grimes, *J. Phys. Chem. C* 113, 6327 (**2009**).
21. O. K. Varghese, M. Paulose, T. J. LaTempa, and C. A. Grimes, *Nano Lett.* 9, 731 (**2009**).
22. S. C. Roy, O. K. Varghese, M. Paulose, and C. A. Grimes, *ACS Nano* 4, 1259 (**2010**).
23. K. Shankar, G. K. Mor, H. E. Prakasam, S. Yoriya, M. Paulose, O. K. Varghese, and C. A. Grimes, *Nanotechnology* 18 (**2007**).
24. O. K. Varghese, M. Paulose, K. Shankar, G. K. Mor, and C. A. Grimes, *J. Nanosci. Nanotechnol.* 5, 1158 (**2005**).
25. X. H. Lu, G. M. Wang, T. Zhai, M. H. Yu, J. Y. Gan, Y. X. Tong, and Y. Li, *Nano Lett.* 12, 1690 (**2012**).
26. K. Shankar, G. K. Mor, M. Paulose, O. K. Varghese, and C. A. Grimes, *J. Non-Cryst. Solids* 354, 2767 (**2008**).
27. S. Kim, G. K. Mor, M. Paulose, O. K. Varghese, K. Shankar, and C. A. Grimes, *IEEE J. Sel. Top. Quantum Electron.* 16, 1573 (**2010**).
28. J. Bandara, K. Shankar, J. Basham, H. Wietasch, M. Paulose, O. K. Varghese, C. A. Grimes, and M. Thelakkat, *Eur. Phys. J.-Appl. Phys.* 53 (**2011**).
29. C. W. Lai, S. Sreekantan, and Z. Lockman, *J. Nanosci. Nanotechnol.* 12, 4057 (**2012**).
30. J. Y. Kim, J. H. Noh, K. Zhu, A. F. Halverson, N. R. Neale, S. Park, K. S. Hong, and A. J. Frank, *ACS Nano* 5, 2647 (**2011**).
31. G. K. Mor, O. K. Varghese, M. Paulose, and C. A. Grimes, *Advanced Functional Materials* 15, 1291 (**2005**).
32. J. Weickert, C. Palumbiny, M. Nedelcu, T. Bein, and L. Schmidt-Mende, *Chemistry of Materials* 23, 155 (**2011**).
33. S. Biswas, M. Shahjahan, M. F. Hossain, and T. Takahashi, *Electrochemistry Communications* 12, 668 (**2010**).
34. O. K. Varghese, M. Paulose, and C. A. Grimes, *Nature Nanotechnology* 4, 592 (**2009**).
35. J. M. Macak, H. Tsuchiya, S. Berger, S. Bauer, S. Fujimoto, and P. Schmuki, *Chemical Physics Letters* 428, 421 (**2006**).
36. T. Yuxin, T. Jie, D. Zhili, O. J. Tien, and C. Zhong, *Advances in Natural Sciences: Nanoscience and Nanotechnology* 2, 045002 (**2011**).
37. V. Galstyan, A. Vomiero, E. Comini, G. Faglia, and G. Sberveglieri, *Rsc Advances* 1, 1038 (**2011**).
38. J. Tao, T. Wu, and P. Gao, *J. Nanosci. Nanotechnol.* 12, 1852 (**2012**).
39. A. Vomiero, V. Galstyan, A. Braga, I. Concina, M. Brisotto, E. Bontempi, and G. Sberveglieri, *Energy and Environmental Science* 4, 3408 (**2011**).
40. P. Xiao, Y. H. Zhang, B. B. Garcia, S. Sepehri, D. W. Liu, and G. Z. Cao, *J. Nanosci. Nanotechnol.* 9, 2426 (**2009**).

41. F. S. Ohuchi and S. C. Freilich, *Journal of Vacuum Science and Technology A: Vacuum, Surfaces, and Films* 4, 1039 **(1986)**.
42. A. Z. Sadek, H. D. Zheng, K. Latham, W. Wlodarski, and K. Kalantar-Zadeh, *Langmuir* 25, 509 **(2009)**.
43. X. F. Yu, Y. X. Li, W. Wlodarski, S. Kandasamy, and K. Kalantar-Zadeh, *Sensors and Actuators B-Chemical* 130, 25 **(2008)**.
44. H. D. Zheng, A. Z. Sadek, M. Breedon, D. Yao, K. Latham, J. du Plessis, and K. Kalantar-Zadeh, *Electrochemistry Communications* 11, 1308 **(2009)**.
45. J. A. Thornton and D. W. Hoffman, *Journal of Vacuum Science and Technology* 14, 164 **(1977)**.
46. F. M. Dheurle and J. M. E. Harper, *Thin Solid Films* 171, 81 **(1989)**.
47. J. C. Manifacier, J. Gasiot, and J. P. Fillard, *Journal of Physics E-Scientific Instruments* 9, 1002 **(1976)**.
48. R. Swanepoel, *Journal of Physics E-Scientific Instruments* 16, 1214 **(1983)**.
49. J. M. Gonzalez-Leal, R. Prieto-Alcon, J. A. Angel, D. A. Minkov, and E. Marquez, *Appl. Optics* 41, 7300 **(2002)**.
50. K. S. Mun, S. D. Alvarez, W. Y. Choi, and M. J. Sailor, *ACS Nano* 4, 2070 **(2010)**.
51. D. A. Wang, L. F. Liu, F. X. Zhang, K. Tao, E. Pippel, and K. Domen, *Nano Lett.* 11, 3649 **(2011)**.

Received: 27 October 2012. Accepted: 23 November 2012.